

Lanthanoid metal nitrates with hydrogen bonded hexamethylenetetramine

Preparation, characterization and kinetics of thermolysis

Dinesh Kumar · I. P. S. Kapoor · Gurdip Singh ·
Udai P. Singh · Nidhi Goel

Received: 20 June 2012 / Accepted: 13 November 2012 / Published online: 20 December 2012
© Akadémiai Kiadó, Budapest, Hungary 2012

Abstract Cerium, praseodymium, and neodymium nitrate complexes with hydrogen bonded hexamethylenetetramine (HMTA) of the formula $[\text{Ce}(\text{NO}_3)_2(\text{H}_2\text{O})_5](\text{HMTA})_2(\text{NO}_3)(\text{H}_2\text{O})_3$, $[\text{Pr}(\text{NO}_3)_2(\text{H}_2\text{O})_6]_2[\text{Pr}(\text{H}_2\text{O})_9](\text{HMTA})_6(\text{NO}_3)_6(\text{H}_2\text{O})_4$ and $[\text{Nd}(\text{NO}_3)_2(\text{H}_2\text{O})_5](\text{HMTA})_2(\text{NO}_3)(\text{H}_2\text{O})_3$ have been prepared and characterized by X-ray crystallography. All the complexes belong to monoclinic crystal system. Ce and Nd complexes have $P21/n$ space group, whereas Pr complex has $C2/c$. Thermal analyses of these complexes were carried out using TG, DSC, which showed their multi-step decomposition. Kinetics of thermolysis has been done by applying model fitting as well as model free isoconversional method. In order to see the response of rapid heating, ignition delay measurements were carried out. The thermal decomposition pathways have also been demonstrated. On the basis of thermal studies the thermal stability of the complexes was found in the order; $\text{Pr} > \text{Ce} > \text{Nd}$. In order to identify the end products of thermolyses, X-ray diffraction patterns of end product were carried out which showed the formation of corresponding metal oxides.

Keywords Hexamethylenetetramine · Ignition delay · Isothermal TG · Kinetics · Lanthanoid metal nitrate · X-ray crystallography

Introduction

The lanthanide (Ln) chemistry is a field of science, which has perceived much attention in the recent years because of their huge and versatile applications [1–5]. Their important feature is a relatively steady variation of properties across the group, which results from the “lanthanoid contraction.” This affects the coordination numbers (CN) and the geometry of their complexes. In few cases the CN of Ln^{n+} ions have been seen nine and ten in which nitrate acts as a bidentate ligand. The most common ligands existing in lanthanide compounds are those one containing oxygen atom. Hexamethylenetetramine (HMTA) is a nitrogen-containing ligand that can coordinate with various metal ions [6, 7]. HMTA is known as urotropine in which four nitrogen atoms constitute a tetrahedron, is a ligand of polycyclicpolydentate type. In many complexes, it acts as a monodentate [8–10] or bidentate bridging ligands [11, 12], and shows non-chelating behavior [13] (in low valent organometallic complexes). Recent progress on the construction of Ag(I)–HMTA networks, including the interesting topologies, synthetic approaches and the important factors that influence the structures, as well as some designed assembly approaches was summarized by Zheng et al. [14]. As a very good hydrogen acceptor, HMTA forms a variety of molecular adducts with hydrogen-donor groups via hydrogen bonding with organic molecules [14]. On the other hand, as a simple and potential tetradentate ligand, it exhibits different coordination modes including the monodentate and μ_n -bridging ($n = 2–4$) modes in ligating metal ions, hence generating a large amount of metal–HMTA complexes.

It is a precursor for the production of various stuffs like antibacterial agents, adhesives, coatings, dye fixatives, anticorrosive agents as well as powerful explosives [15]. Very recently Cheng et al. [16] have reported that HMTA acts both as a ligand and a reducing agent in AGET atom

D. Kumar · I. P. S. Kapoor · G. Singh (✉)
Department of Chemistry, DDU Gorakhpur University,
Gorakhpur 273 009, India
e-mail: gsingh4us@yahoo.com

U. P. Singh · N. Goel
Department of Chemistry, Indian Institute of Technology
Roorkee, Roorkee 247 667, India

transfer radical batch emulsion polymerization. Thermal, structural, and spectroscopic properties of magnesium sulfate complexes with HMTA and 1,10-phenanthroline were also investigated by another group [17]. Hence, HMTA has been a versatile candidate for research and is a target for different research groups. Konar et al. [18] have reported the synthesis of two new 1D and 3D networks of Cu(II) and Co(II) using malonate and HMTA as bridging ligands. Simultaneous determination of Pt and Rh by catalytic adsorptive stripping voltammetry, using HMTA as complexing agent was investigated by Dalvi et al. [19].

Preparation was carried out by following method at room temperature. Solid HMTA was mixed with metal nitrates hexa-hydrates (solid) followed by the addition of water in 1:1 ratio (by mass). The reaction contents were shaken well till the formation of homogeneous solution. This homogeneous solution after filtration was kept for crystal growth and crystallized complexes were further recrystallized from water to get the single crystals. The obtained crystals were characterized by X-ray crystallography.



In metal amine nitrate complexes, the presence of nitrate (an oxidizing group) leads to their various applications such as in explosives, propellants, and pyrotechnics [20, 21] and display exothermic decompositions at elevated temperatures. While decomposition, these explosives produce energy by a process called oxidation. During the oxidation reaction, an explosive is detonated with sudden release of energy or a fuel is burnt. The oxidation reaction produces heat because the internal energy of reactant molecule is higher than that of the end product.

Moreover, these complexes are being used as potential burning rate modifier for HTPB-AP solid propellants [22, 23]. In addition, these complexes are also used to obtain ultrafine metal oxides.

Recently, we have undertaken thermal studies on some transition metal nitrate and perchlorate complexes with HMTA in which it was attached to metal ion through H-bonding [24, 25]. Similar other complexes with various ligands have also been prepared by our group and subjected for similar investigation [26–29]. Recently, Trzesowski-Kruszynska et al. [30] have investigated coordination sphere geometry changes of lanthanoid (III) nitrate complexes with HMTA. Thermal behavior of hydrogen bonded HMTA Lanthanoid metal nitrate complexes has not been reported in literature. Based on the above considerations, present investigation deals with preparation, X-ray crystallography, and kinetic of thermolysis of Lanthanoid metal nitrate complexes with hydrogen bonded HMTA. The reported complexes have CN nine and ten.

Experimental

Materials and methods

All the chemicals were obtained from different commercial suppliers such as CDH (metal nitrates) and Lancaster (HMTA) and used without further purification.

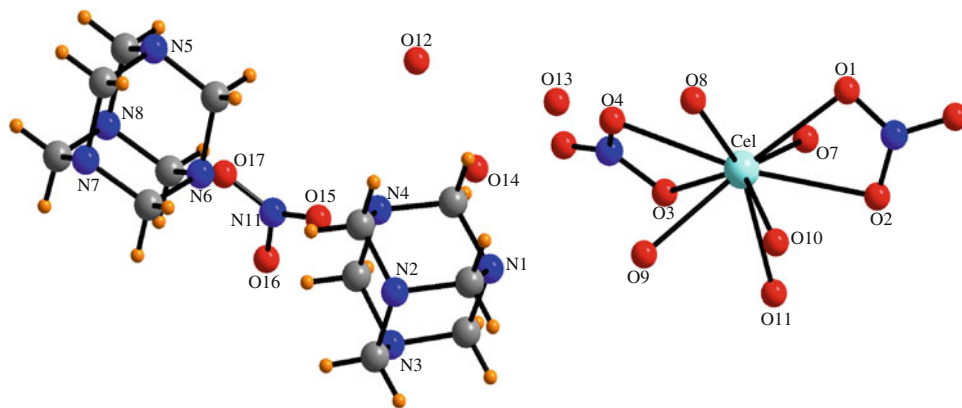
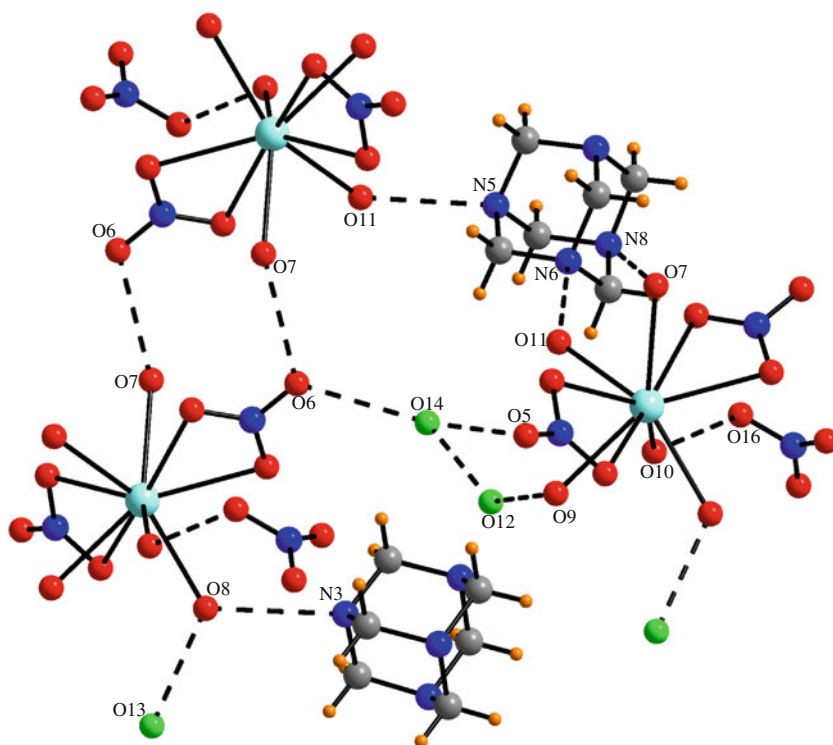
where M = Ce, Pr, and Nd.

Determination of crystal structure

The X-ray data collection were performed on a Bruker Kappa Apex four circle-CCD diffractometer using graphite monochromated Mo-K_α radiation ($\lambda = 0.71070 \text{ \AA}$) at 296 K. In the reduction of data Lorentz and polarization corrections, empirical absorption corrections were applied [31]. Crystal structures were solved by direct methods. Structure solution, refinement, and data output were carried out with the SHELXTL program [32, 33]. Non-hydrogen atoms were refined anisotropically. Hydrogen atoms were placed in geometrically calculated positions by a riding model. Images and Hydrogen bonding interactions were created in the crystal lattice with DIAMOND and MERCURY software [34, 35]. Molecular structures, various non-covalent interactions, and three-dimensional views of these complexes have been shown in Figs. 1–9. The crystallographic data, structure refinement parameters, bond length, and bond angles are given in Tables 1 and 2.

Thermal analysis

Thermogravimetry and differential scanning calorimetry (TG-DSC) (Fig. 10; Table 3) of studied complexes were undertaken at $10 \text{ }^\circ\text{C min}^{-1}$ (sample mass = 2.8 mg, 100–200 mess) under nitrogen atmosphere at the flow rate of 200 mL min^{-1} on Perkin Elmer (Pyris Diamond) instrument (Fig. 10). Corresponding metal oxides as end product of thermolysis were revealed by their X-ray diffraction (XRD) patterns (Fig. 11). Isothermal TG (sample mass = 20 mg, 100–200 mess) was performed to study the kinetics of their isothermal decomposition at appropriate temperatures in static air (mass ~ 20 mg) with indigenously fabricated TG

Fig. 1 Molecular structure of Ce complex**Fig. 2** Various non-covalent interactions in Ce complex

apparatus [36]. Gold crucible was used as a sample holder throughout the isothermal TG experiments.

Kinetic analysis of isothermal TG data

Following single step kinetic equation (Eq. 1) pertains the kinetic analysis of thermal decomposition of a solid [37].

$$d\alpha/dt = k(T) \cdot f(\alpha) \quad (1)$$

where t is the time, T is the temperature, α is the extent of conversion ($0 < \alpha < 1$), $k(T)$ is the rate constant, and $f(\alpha)$ is the reaction model [37], which describes the dependence of the reaction rate on the extent of reactions. The value of α is

experimentally derived from the mass loss in TG experiments. The reaction model may take various forms. The temperature dependence of $k(T)$ could be described by the Arrhenius equation which on substitution into Eq. (1) yields

$$d\alpha/dt = A \exp(-E/RT) \cdot f(\alpha) \quad (2)$$

where A is pre-exponential factor, E activation energy, and R the gas constant.

Model fitting method

If we rearrange and integrate Eq. (1) for isothermal conditions then it turns out that

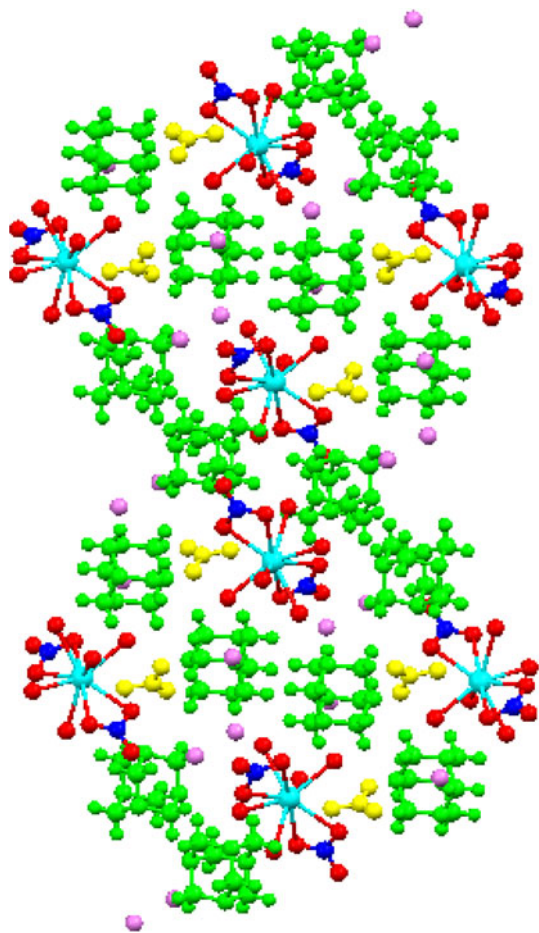
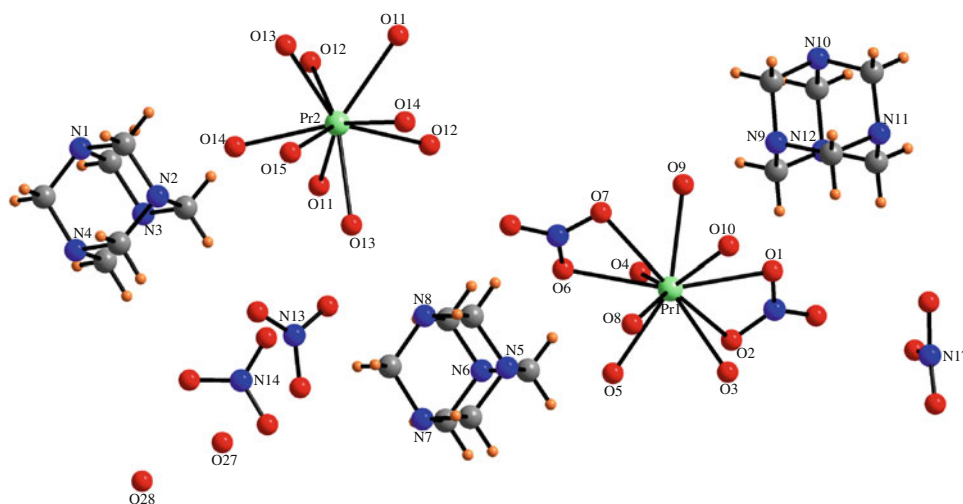


Fig. 3 Three-dimensional view in Ce complex

$$g_j(\alpha) = k_j(T)t \quad (3)$$

where $g(\alpha) = \int_0^\alpha [f(\alpha)]^{-1} d\alpha$ denotes the integrated form of the reaction model [29]. The subscript j has been used to emphasize that on substituting a particular reaction model

Fig. 4 Molecular structure of Pr complex



in Eq. (3) results in evaluating the corresponding rate constant, which is determined from the slope of a plot of $g_j(\alpha)$ versus t . In this method for each reaction model selected, the rate constants are evaluated at several temperatures T_i and Arrhenius parameters are determined (Table 4) using the Arrhenius equation (4) in its logarithmic form using isothermal TG experimental data.

$$\ln k_j(T_i) = \ln A_j - E_j/RT_i. \quad (4)$$

Isoconversional method

This method persists the calculation of activation energy without making any assumptions about the reaction model. In addition, this method evaluates the effective activation energy as a function of the extent of conversion (Fig. 12) which allows one to explore multistep kinetics.

In isoconversional method [38], it is assumed that the reaction model as defined in Eq. (1) is not dependent on temperature or heating rate. Under isothermal conditions, on combining Eqs. (3) and (4) we get,

$$-\ln t_{\alpha,i} = \ln [A_\alpha/g(\alpha)] - E_\alpha/RT_i \quad (5)$$

where E_α could be evaluated from the slope of the plot of $-\ln t_{\alpha,i}$ against T_i^{-1} .

Ignition delay (D_i) measurements

Their responses to sudden heating conditions were observed by ignition delay (D_i) measurements, recorded using tube furnace technique [39] (sample mass ~ 20 mg) in the temperature range of 330–430 °C (Table 5). The accuracy of the temperature of tube furnace was ± 1 °C. Furthermore, same aspect was used to study the correlation of ignition time (D_i or t_{id}) with activation energy as reported by Singh et al. [25, 26]. A plot which is indicative of variation of ignition time against $1/T$ (K) is apparent in Fig. 13.

Results and discussion

Structure description

The Ce complex has the monoclinic crystal system with space group $P2_1/n$ ($Z = 4$) and its molecular structure is shown in Fig. 1. Cerium atom is nine coordinated, which is achieved by nine oxygen atoms, i.e., four oxygen atoms (O1, O2, O3, and O4) from two bidentate nitrate groups and five from five water molecules (O7, O8, O9, O10, and O11). The structure also contains one nitrate ion, three water molecules, and two HMTA moieties in the lattice. Hence this complex could be formulated as $[\text{Ce}(\text{NO}_3)_2(\text{H}_2\text{O})_5](\text{HMTA})_2(\text{NO}_3)(\text{H}_2\text{O})_3$. The Ce–O bond distances are in the range of 2.483(4)–2.738(6) Å.

The Ce1–O1 to Ce1–O4 bond distances are greater than Ce1–O7 to Ce1–O11, due to the higher electronegativity of nitrogen atom of nitrates which pulls the electron itself and increases the Ce1–O1 to Ce1–O4 bond distance. The crystal packing shows the various non-covalent O...O [O5...O14, 2.637(16) Å; O6...O7, 2.850(8) Å; O6...O14, 2.784(12) Å; O8...O13, 2.747(8) Å; O9...O12, 2.752(15) Å; O10...O16, 2.813(11) Å; O12...O14, 2.416(2) Å] and N...O [N3...O8, 2.858(7) Å; N5...O11, 2.784(5) Å; N6...O11, 2.871(5) Å; N8...O7, 2.883(5) Å] interactions with each other to give a three-dimensional dumbbell like view (Figs. 2, 3).

The Pr complex crystallizes in monoclinic system and having the $C2/c$ space group ($Z = 4$). As shown in Fig. 4, it is clear that this complex contains two type of Pr atom,

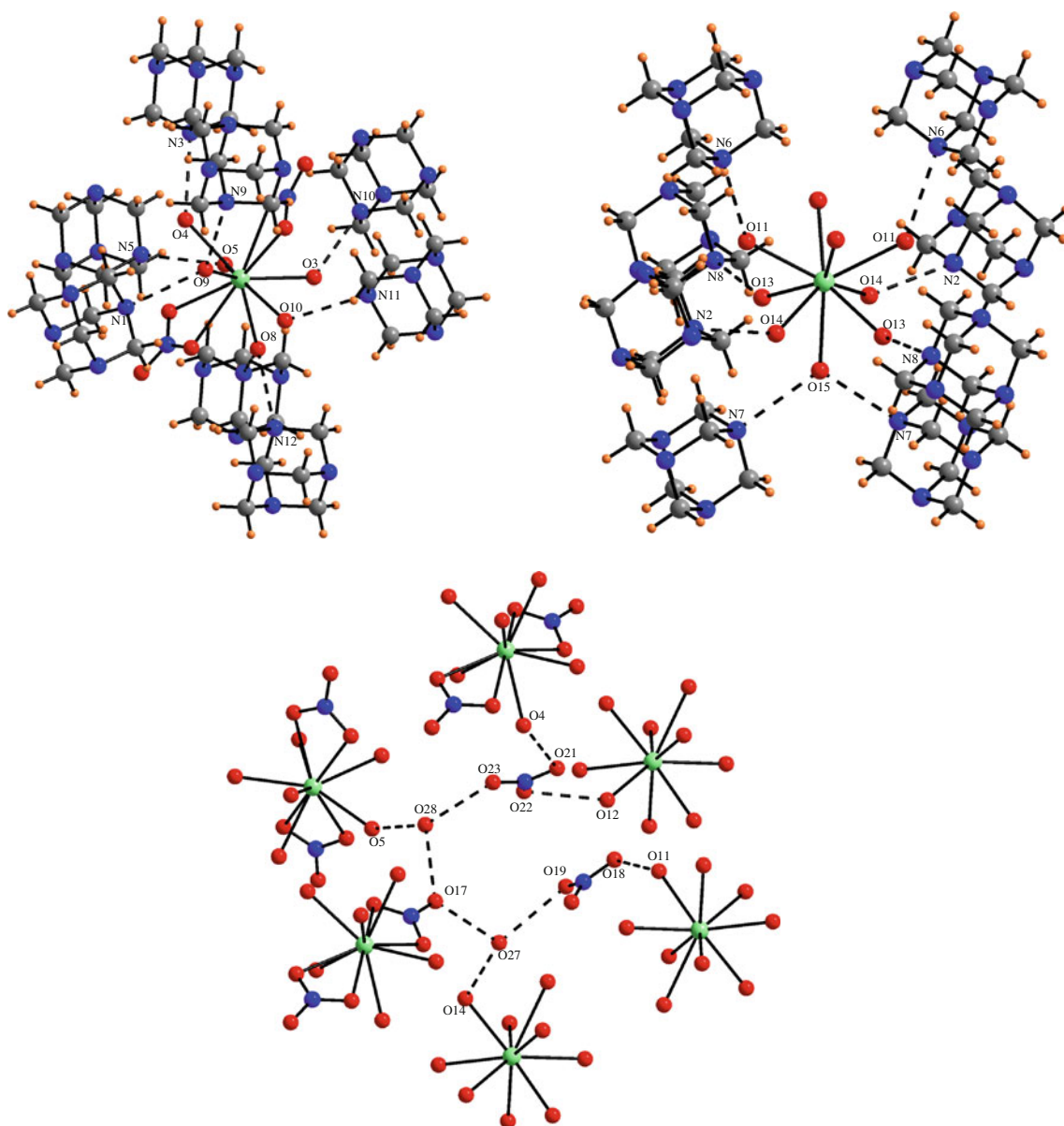


Fig. 5 Various non-covalent interactions in Pr complex

Fig. 6 Three-dimensional sheet like view in Pr complex

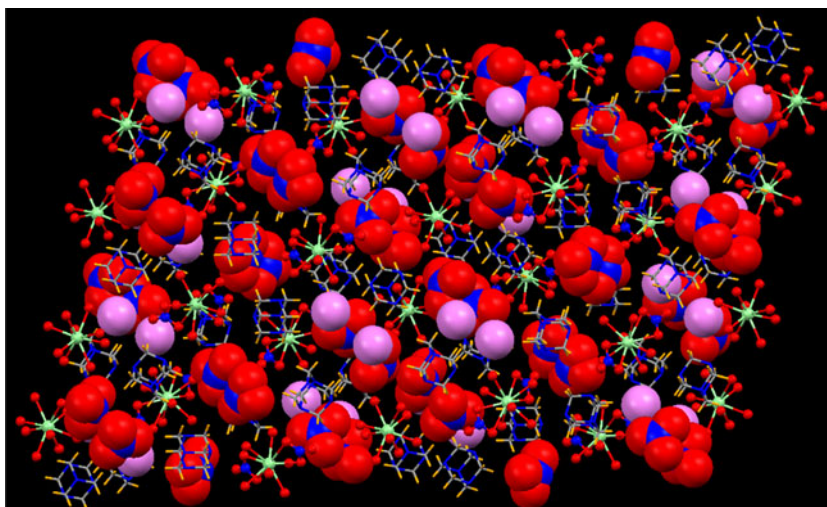
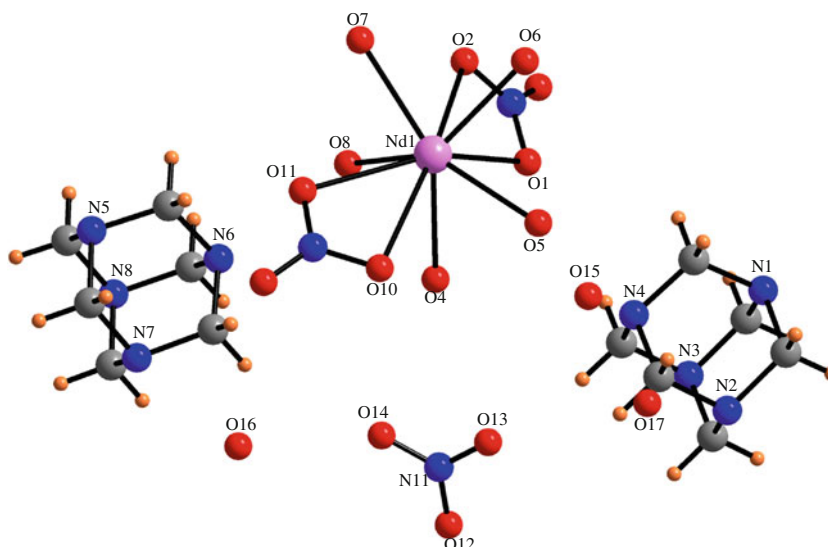


Fig. 7 Molecular structure of Nd complex



first one is ten coordinated and the other is nine coordinated. The first Pr1 center is coordinated through ten oxygen atoms, among those six are coming from water molecules (O3, O4, O5, O8, O9, and O10) and four from bidentate nitrate ion (O1, O2, O6, and O7), whereas second Pr2 completes its coordination through nine oxygen atoms, of water molecules. This structure also contains six uncoordinated nitrate ions, six HMTA moieties, and four water molecules. The molecule could be represented as; $[\text{Pr}(\text{NO}_3)_2(\text{H}_2\text{O})_6]_2[\text{Pr}(\text{H}_2\text{O})_9](\text{HMTA})_6(\text{NO}_3)_6(\text{H}_2\text{O})_4$.

The crystal packing shows the various non-covalent O...O [O4...O21, 2.989(9) Å; O5...O28, 2.741(6) Å; O11...O18, 2.888(6) Å; O12...O22, 2.849(8) Å; O14...O27, 2.751(8) Å; O17...O27, 2.830(6) Å; O17...O28, 2.796(10) Å; O19...O27, 2.778(8) Å; O23...O28, 2.863(11) Å] and N...O [N1...O9,

2.894(8) Å; N2...O14, 2.858(10) Å; N3...O4, 2.921(9) Å; N5...O5, 2.882(5) Å; N6...O11, 2.825(7) Å; N7...O15, 2.878(10) Å; N8...O13, 2.739(7) Å; N9...O9, 2.879(8) Å; N10...O3, 2.865(7) Å; N11...O10, 2.775(6) Å; N12...O8, 2.903(10) Å] interactions with each other to give a three-dimensional sheet like view (Figs. 5, 6).

The molecular structure of Nd complex is similar to Ce complex (Fig. 7). This also crystallizes in the monoclinic crystal system with space group $P2_1/n$ ($Z = 4$). The formulation of this molecule could be $[\text{Nd}(\text{NO}_3)_2(\text{H}_2\text{O})_5](\text{HMTA})_2(-\text{NO}_3)(\text{H}_2\text{O})_3$. The crystal packing gives three-dimensional sheet like view through various non-covalent O...O [O3...O17, 2.820(1) Å; O4...O14, 2.999(10) Å; O5...O16, 2.749(8) Å; O6...O14, 2.854(11) Å; O9...O17, 2.720(14) Å; O12...O16, 2.952(24) Å; O15...O17, 2.259(19) Å] and N...O [N1...O16, 2.921(7) Å; N2...O6, 2.811(9) Å; N4...O5, 2.863(10) Å;

Fig. 8 Various non-covalent interactions in Nd complex

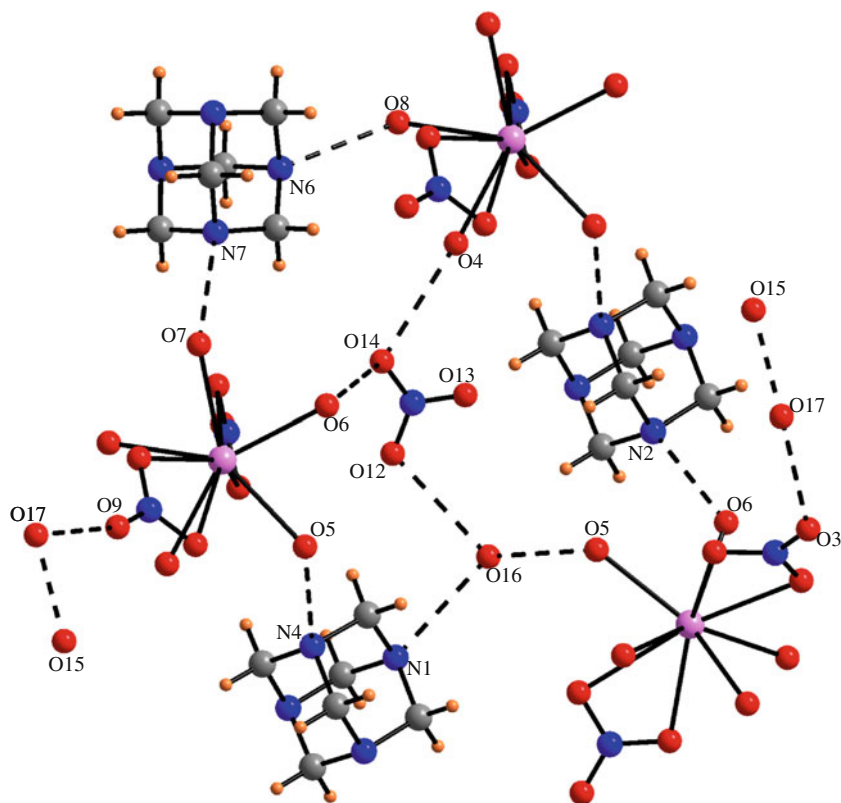
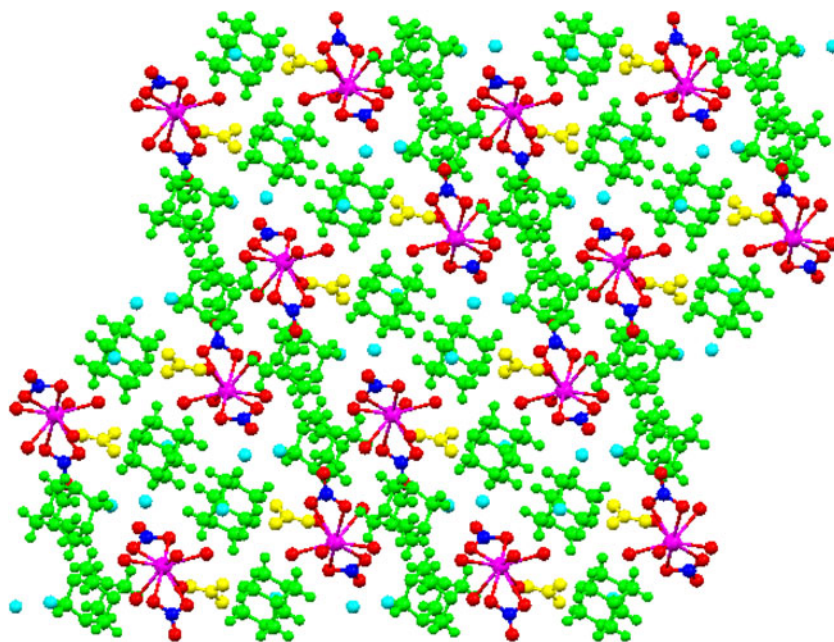


Fig. 9 Three-dimensional view in Nd complex



$N6 \cdots O8$, 2.898(5) Å; $N7 \cdots O7$, 2.873(7) Å] interactions (Figs. 8, 9).

Thermal analysis

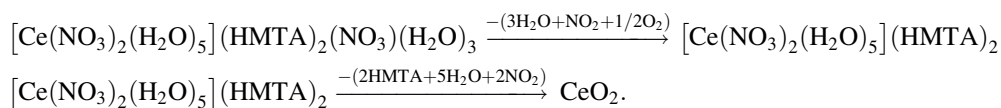
From the TG-DSC traces of characterized complexes it turns out that these follow multi-step decomposition

pathways. The cerium complex decomposes in two steps (Fig. 10). The TG-DSC traces show two regions of mass loss: (i) around 15.5 % mass loss in the 55–140 °C region (which is due to the loss of three non-coordinated water molecules and one non-coordinated nitrate group), (ii) around 62.0 % mass loss in 180–500 °C region (which is due to the loss of two HMTA, five water and two nitrate

Table 1 Crystallographic data and refinement details for nitrate complexes

Complex designation	Ce	Pr	Nd
Formula	C ₁₂ H ₂₄ N ₁₁ O ₁₇ Ce	C ₃₆ H ₇₂ N ₃₄ O ₅₅ Pr ₃	C ₁₂ H ₂₄ N ₁₁ O ₁₇ Nd
Colors	Colorless	Green	Purple
Molecular mass	734.54	2284.01	738.66
Temp/K	296/2	296/2	296/2
$\lambda/\text{\AA}$	0.71073	0.71073	0.71073
Crystal system	Monoclinic	Monoclinic	Monoclinic
Space group	<i>P21/n</i>	<i>C2/c</i>	<i>P21/n</i>
Unit dimensions	$a = 17.942/4 \text{ \AA}, \alpha = 90.00^\circ$ $b = 9.4018/2 \text{ \AA}, \beta = 111.97/10^\circ$ $c = 18.5699/4 \text{ \AA}, \gamma = 90.00^\circ$	$a = 51.342/5 \text{ \AA}, \alpha = 90.00^\circ$ $b = 10.423/5 \text{ \AA}, \beta = 103.98/5^\circ$ $c = 16.970/5 \text{ \AA}, \gamma = 90.00^\circ$	$a = 17.8745/17 \text{ \AA}, \alpha = 90.00^\circ$ $b = 9.3981/8 \text{ \AA}, \beta = 111.77/4^\circ$ $c = 18.5010/17 \text{ \AA}, \gamma = 90.00^\circ$
Volume	2904.85/11 A ³	8812/5 A ³	2886.1/5 A ³
Molecules per unit cell, <i>Z</i>	4	4	4
Density/ <i>D_x</i>	1.723 Mg m ⁻³	1.723 Mg m ⁻³	1.700 Mg m ⁻³
Absorption coefficient	1.680 Mg m ⁻³	1.753 mm ⁻¹	1.888 mm ⁻¹
Diffractometer used	Bruker Kappa Apex	Bruker Kappa Apex	Bruker Kappa Apex
Crystal size	0.33 × 0.25 × 0.17 mm ³	0.34 × 0.26 × 0.19 mm ³	0.29 × 0.22 × 0.14 mm ³
θ range	2.00–33.12°	0.82–33.73°	1.35–32.80°
Refinement method	Full matrix least-square on <i>F</i> ²	Full matrix least-square on <i>F</i> ²	Full matrix least-square on <i>F</i> ²
Radiation	Mo-K _{α}	Mo-K _{α}	Mo-K _{α}
Goodness-off-fit on <i>F</i> ²	1.920	0.653	1.944
Final <i>R</i> indices [<i>I</i> > 2σ(<i>I</i>)]	0.0680	0.0377	0.0654
CCDC No.	840405	840404	840403

groups) resulting the oxidation of metal and formation of cerium oxide. These regions corresponds an endotherm and an exotherm in the DSC traces (Table 3). In our previous studies [25–29], we have found metal oxide as the end product after thermal decomposition of the transition metal amine nitrates. Similar case was also observed and cerium oxide (CeO₂) as end product was inferred by the (111) peak of maximum intensity XRD patterns (Fig. 11). The decomposition pathways for cerium complex may be generalized as:



(~16.5 % mass loss), which is due to the loss of five non-coordinated water molecules and four non-coordinated nitrate groups. After this the residue remains no longer stable and second step mass loss occurs in the 190–500 °C region (~60.0 % mass loss) which is due to the loss of twelve HMTA, twenty six water molecules and nine nitrate groups resulting the oxidation of metal and formation of praseodymium oxide (Pr₆O₁₁) as a residue which is evident from (111) peak of maximum intensity in the XRD pattern (Fig. 11). Corre-

Praseodymium complex also follows the same pattern, i.e., two steps decomposition. The first step decomposition occurs in the temperature range of 70–140 °C

responding to these regions an endotherm at 135 °C and an exotherm at 268 °C were noticed in DSC traces (Table 3).

Table 2 Selected bond lengths and angles for nitrate complexes

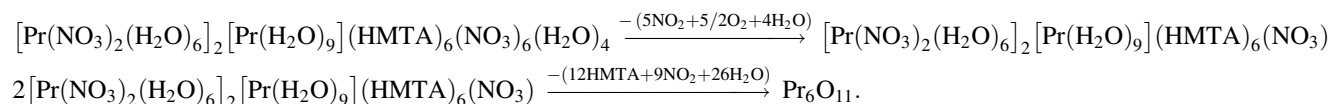
Ce				Pr				Nd			
Bond	Length	Bond	Angle	Bond	Length	Bond	Angle	Bond	Length	Bond	Angle
Ce1–O11	2.483/4	O11–Ce1–O8	146.07/14	Pr1–O8	2.492/3	O8–Pr1–O10	72.01/9	Nd1–O7	2.456/4	O7–Nd1–O6	76.84/15
Ce1–O8	2.497/6	O11–Ce1–O10	76.66/14	Pr1–O1	2.503/8	O8–Pr1–O5	78.07/9	Nd1–O6	2.462/5	O7–Nd1–O5	146.10/15
Ce1–O10	2.503/5	O8–Ce1–O10	74.03/17	Pr1–O5	2.511/8	O10–Pr1–O5	145.39/9	Nd1–O5	2.461/7	O6–Nd1–O5	73.89/17
Ce1–O9	2.548/4	O11–Ce1–O9	76.50/15	Pr1–O3	2.528/6	O8–Pr1–O3	69.16/7	Nd1–O4	2.512/5	O7–Nd1–O4	141.41/13
Ce1–O7	2.564/4	O8–Ce1–O9	77.39/17	Pr1–O9	2.530/6	O10–Pr1–O3	76.64/9	Nd1–O8	2.530/5	O6–Nd1–O4	136.33/14
Ce1–O3	2.579/5	O10–Ce1–O9	69.15/17	Pr1–O4	2.532/8	O5–Pr1–O3	76.77/9	Nd1–O11	2.547/6	O5–Nd1–O4	72.41/16
Ce1–O1	2.644/3	O11–Ce1–O7	75.68/12	Pr1–O6	2.571/6	O8–Pr1–O9	124.83/9	Nd1–O1	2.604/8	O7–Nd1–O8	75.78/12
Ce1–O2	2.679/4	O8–Ce1–O7	137.71/15	Pr1–O1	2.576/7	O10–Pr1–O9	73.95/9	Nd1–O2	2.666/5	O6–Nd1–O8	132.03/15
Ce1–O4	2.736/6	O10–Ce1–O7	132.12/15	Pr1–O2	2.624/7	O5–Pr1–O9	139.47/9	Nd1–O10	2.735/6	O5–Nd1–O8	137.55/15
		O9–Ce1–O7	137.91/13	Pr1–O7	2.785/7	O3–Pr1–O9	139.61/9			O4–Nd1–O8	66.70/12
		O11–Ce1–O3	72.88/14	Pr2–O14 ⁱ	2.486/7	O8–Pr1–O4	140.57/9			O7–Nd1–O11	73.72/14
		O8–Ce1–O3	119.01/17	Pr2–O14	2.486/7	O10–Pr1–O4	142.51/10			O6–Nd1–O11	136.17/16
		O10–Ce1–O3	135.83/17	Pr2–O13	2.501/6	O5–Pr1–O4	71.94/10			O5–Nd1–O11	118.05/17
		O9–Ce1–O3	73.15/17	Pr2–O13 ⁱ	2.501/6	O3–Pr1–O4	125.57/10			O4–Nd1–O11	84.86/15
		O7–Ce1–O3	68.84/15	Pr2–O11	2.525/9	O9–Pr1–O4	70.66/10			O8–Nd1–O11	69.72/14
		O11–Ce1–O1	114.15/11	Pr2–O11 ⁱ	2.525/9	O10–Pr1–O6	118.43/9			O7–Nd1–O1	114.31/11
		O8–Ce1–O1	76.28/14	Pr2–O12	2.532/7	O5–Pr1–O6	66.98/10			O6–Nd1–O1	78.35/15
		O10–Ce1–O1	78.61/14	Pr2–O12 ⁱ	2.532/7	O3–Pr1–O6	131.96/10			O5–Nd1–O1	76.01/14
		O9–Ce1–O1	142.79/13	Pr2–O15	2.646/3	O9–Pr1–O6	86.85/11			O4–Nd1–O1	67.19/13
		O7–Ce1–O1	78.16/12			O4–Pr1–O6	71.77/11			O8–Nd1–O1	78.14/12
		O3–Ce1–O1	143.49/14			O8–Pr1–O1	131.71/9			O11–Nd1–O1	143.87/14
		O11–Ce1–O2	66.56/12			O10–Pr1–O1	69.72/9			O7–Nd1–O2	66.26/12
		O8–Ce1–O2	115.91/15			O5–Pr1–O1	122.68/9			O6–Nd1–O2	67.74/15
		O10–Ce1–O2	67.74/14			O3–Pr1–O1	74.23/9			O5–Nd1–O2	116.13/16
		O9–Ce1–O2	128.03/13			O4–Pr1–O1	86.72/10			O4–Nd1–O2	104.00/13
		O7–Ce1–O2	65.61/12			O6–Pr1–O1	152.75/10			O8–Nd1–O2	65.38/14
		O3–Ce1–O2	124.45/15			O10–Pr1–O2	113.14/9			O11–Nd1–O2	125.19/15
		O1–Ce1–O2	47.59/11			O5–Pr1–O2	74.39/9			O1–Nd1–O2	48.05/13
		O11–Ce1–O4	115.77/14			O3–Pr1–O2	65.26/8			O7–Nd1–O10	115.90/15
		O8–Ce1–O4	70.75/16			O9–Pr1–O2	102.22/9			O6–Nd1–O10	127.17/18
		O10–Ce1–O4	126.48/16			O4–Pr1–O2	64.03/10			O5–Nd1–O10	71.08/17
		O9–Ce1–O4	64.79/16			O8–Pr1–O7	64.47/8			O4–Nd1–O10	64.54/16
		O7–Ce1–O4	100.70/15			O10–Pr1–O7	72.74/9			O8–Nd1–O10	100.20/15
		O3–Ce1–O4	48.50/17			O5–Pr1–O7	109.48/9			O11–Nd1–O10	47.28/17
		O1–Ce1–O4	127.98/14			O9–Pr1–O7	64.66/9			O1–Nd1–O10	127.54/15
		O2–Ce1–O4	165.65/14			O4–Pr1–O7	102.17/10			O2–Nd1–O10	164.97/17
						O1–Pr1–O7	127.07/9				
						O2–Pr1–O7	164.36/9				
						O14 ⁱ –Pr2–O14	133.33/9				
						O14 ⁱ –Pr2–O13	74.06/11				
						O14–Pr2–O13	86.57/11				
						O14 ⁱ –Pr2–O13 ⁱ	86.57/11				
						O14–Pr2–O13 ⁱ	74.06/11				
						O13–Pr2–O13 ⁱ	130.07/10				
						O14 ⁱ –Pr2–O11	69.06/10				
						O14–Pr2–O11	137.02/10				
						O13 ⁱ –Pr2–O11	71.48/9 ⁱ				
						O14 ⁱ –Pr2–O11 ⁱ	137.02/10				
						O14–Pr2–O11 ⁱ	69.06/10				
						O13–Pr2–O11 ⁱ	71.48/9				
						O13 ⁱ –Pr2–O11 ⁱ	135.75/10				

Table 2 continued

Ce				Pr				Nd			
Bond	Length	Bond	Angle	Bond	Length	Bond	Angle	Bond	Length	Bond	Angle
						O14 ⁱ -Pr2-O12	79.55/10				
						O14-Pr2-O12	138.8/1				
						O13-Pr2-O12	79.71/10				
						O13 ⁱ -Pr2-O12	141.92/10				
						O11-Pr2-O12	70.44/10				
						O11 ⁱ -Pr2-O12	69.75/10				
						O14 ⁱ -Pr2-O12 ⁱ	138.8/1				
						O14-Pr2-O12 ⁱ	79.55/10				
						O13-Pr2-O12 ⁱ	141.92/10				
						O13 ⁱ -Pr2-O12 ⁱ	79.71/10 ⁱ				
						O11-Pr2-O12 ⁱ	69.75/10 ⁱ				
						O11 ⁱ -Pr2-O12 ⁱ	70.44/10 ⁱ				
						O12-Pr2-O12 ⁱ	87.74/10				
						O14 ⁱ -Pr2-O15	66.66/7				
						O14-Pr2-O15	66.66/7				
						O13-Pr2-O15	65.04/7				
						O13 ⁱ -Pr2-O15	65.04/7				
						O11-Pr2-O15	118.18/7				
						O11 ⁱ -Pr2-O15	118.18/7				
						O12-Pr2-O15	136.13/7				
						O12 ⁱ -Pr2-O15	136.13/7				

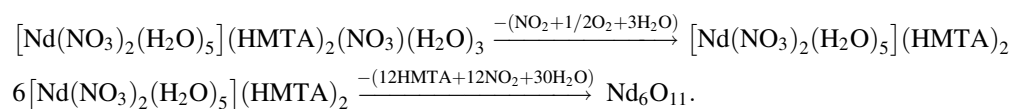
Thus, the decomposition pathways pertaining praseodymium complex may be suggested as:

these parameters activation energy for thermal decomposition were calculated. In this method, the kinetics is ana-



Similar behavior was also shown by the neodymium complex and the neodymium oxide (Nd_6O_{11}) was observed as the end product (Fig. 11). Therefore, its decomposition pathways may also be proposed as:

lyzed by choosing a “best fit” model based on the values of correlation coefficient ‘ r ’ close to 1. Among the various values of ‘ r ’, calculated for different models the higher value of ‘ r ’ corresponds to model 5, 11 and 14 for Ce



In the model fitting method of kinetic analysis, all the 14 kinetic models [29] were applied to the isothermal TG data taken in the temperature range 230–290 °C. Different parameters such as slope, $\ln A$, correlation coefficients etc. were calculated by different models and with the help of

complex (Table 4). Their corresponding values of E_a are respectively 26.0, 27.0, and 26.7(±1) kJ mol^{-1} . For Pr complex models, 12 and 13 shows highest values of ‘ r ’ [24] and corresponding E_a values are 45.4 and 45.0 kJ mol^{-1} . In the case of Nd complex model, 14 shows

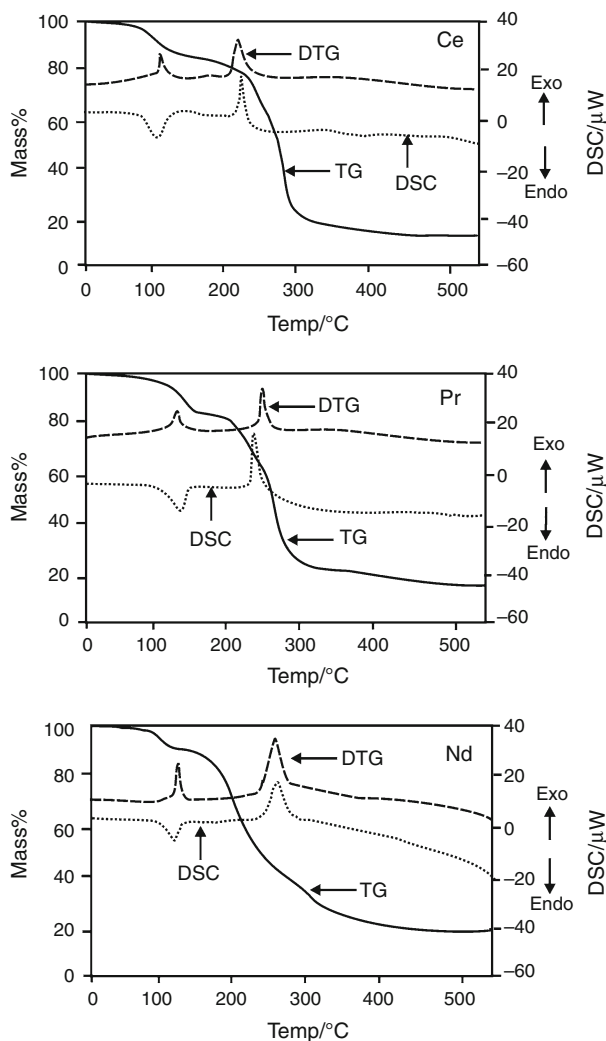


Fig. 10 Non-isothermal TG and DSC traces of complexes in nitrogen

the highest value of ' r ', therefore this is the best fit model for the thermal decomposition of this complex and the corresponding activation energy value is 23.9 kJ mol^{-1} . This method generates different values of activation energy values from each model. These average values are 24.8, 41.6, and 22.1 kJ mol^{-1} for respective complex.

Isoconversional method was applied to the isothermal TG data which indicates that the decomposition of these

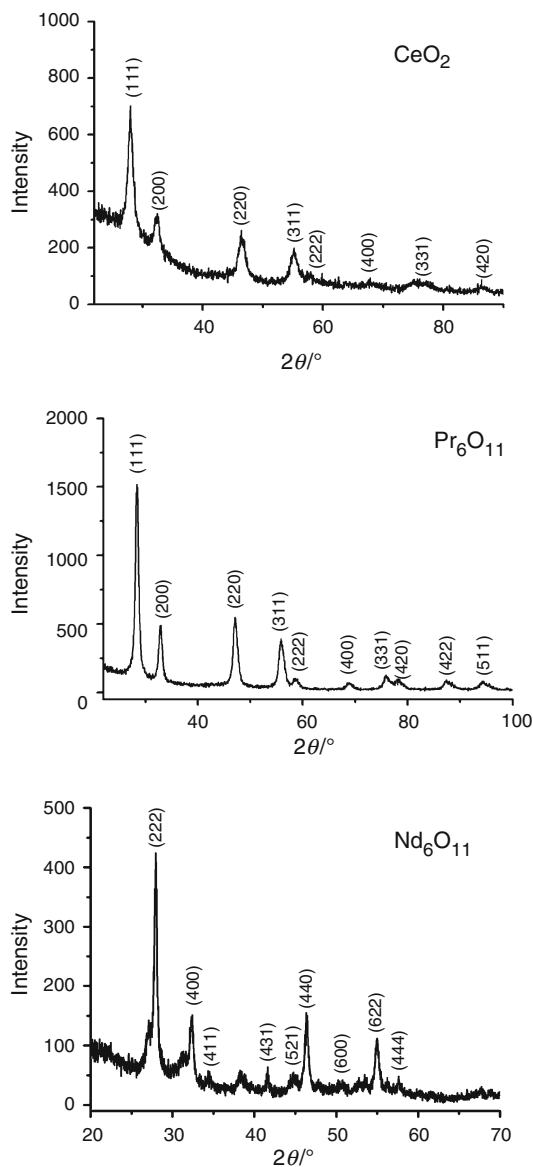


Fig. 11 X-ray diffraction pattern of metal oxides obtained after thermal decomposition of the corresponding complexes

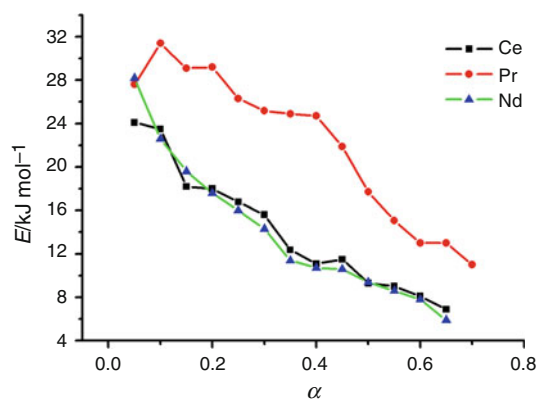
complexes is not simple, as indicated by model fitting methods. Values of E for these complexes are found to vary with α as we have just observed that the removal of

Table 3 TG-DSC data describing the percentage decomposition in different steps, peak position, and nature of peaks for the complexes

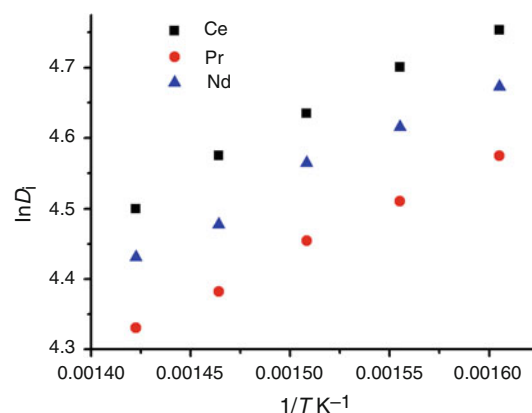
Complex	Step	TG		DSC	
		Temperature range	% Decomposition	Peak position/°C	Exo/endo
Ce	I	55–140	15.5	124	Endo
	II	180–500	62.0	230	Exo/sharp
Pr	I	70–140	16.5	135	Endo
	II	190–500	60.0	268	Exo/sharp
Nd	I	90–144	15.7	132	Endo
	II	170–500	62.5	291	Exo

Table 4 Various kinetic parameters for isothermal decomposition of nitrate complexes

Model	Ce complex			Pr complex			Nd complex		
	$E_a/\text{kJ mol}^{-1}$	$\ln A$	r	$E_a/\text{kJ mol}^{-1}$	$\ln A$	r	$E_a/\text{kJ mol}^{-1}$	$\ln A$	r
1	23.0	0.231	0.9886	39.2	-3.300	0.9474	20.1	1.116	0.9606
2	23.2	0.003	0.9888	39.6	-3.560	0.9488	24.7	-0.034	0.9606
3	22.2	-0.025	0.9472	40.2	-3.912	0.9516	20.7	0.612	0.9645
4	27.6	-1.279	0.9607	43.1	-4.689	0.9649	22.6	0.201	0.9752
5	26.2	-0.705	0.9901	44.2	-4.798	0.9698	23.3	0.230	0.9787
6	25.6	-1.38	0.9898	43.5	-5.434	0.9681	22.7	-0.462	0.9760
7	24.5	-0.529	0.9896	41.5	-4.333	0.9549	21.5	0.384	0.9692
8	23.9	-0.458	0.9891	40.9	-4.205	0.9562	20.3	0.582	0.8978
9	24.4	-0.815	0.9894	27.4	-1.271	0.7522	21.5	0.091	0.9696
10	25.3	-0.031	0.9898	41.6	-4.644	0.9595	22.4	0.889	0.9743
11	27.0	0.727	0.9900	42.9	-4.000	0.9651	23.0	1.873	0.9151
12	25.1	-0.313	0.9898	45.4	-3.560	0.9766	22.2	0.608	0.9734
13	23.4	-1.985	0.9887	45.0	-6.465	0.9763	20.5	-1.100	0.9640
14	26.7	0.994	0.9901	48.6	-7.637	0.9585	23.9	1.923	0.9810

**Fig. 12** Dependence of activation energies (obtained from isoconversional method, E^*) on the extent of conversion (α) for the complexes

different moieties accounted to different alpha values in different steps. Figure 12 represents the dependencies of activation energies. Kinetic analysis performed by isoconversional method on isothermal TG data is consistent with the fact that thermal decomposition of these complexes has initial overall activation energy of 24, 27, and 29 kJ mol^{-1} , respectively. These values changes with the extent of conversion to about 7, 11, and 6 kJ mol^{-1} ,

**Fig. 13** Plot of log of time of ignition ($\ln D_i$) against the reciprocal of the absolute temperature ($1/T$) for the complexes

respectively, for cerium, praseodymium, and neodymium complexes at the end of reactions. For these complexes, variation of E is due to the predominance of exothermic changes over endothermic changes. However, the variation of activation energy with extent of conversion is changing at every stage, which might be the result of many competing effects and is very difficult to correlate particular activation energy for a particular process in the thermolysis of these big molecules.

Table 5 Ignition delay activation energy for thermal explosion (E^*) and correlation coefficient (r) for the nitrate complexes (DNI-Do not ignite)

Complex	D_i/s at temperature/ $^{\circ}\text{C}$						$E^*/\text{kJ mol}^{-1}$	r	$\ln k$
	330 \pm 1	350 \pm 1	370 \pm 1	390 \pm 1	410 \pm 1	430 \pm 1			
Ce	DNI	107	101	96	88	84	11.5	0.9960	2.542
Pr	DNI	116	110	103	97	90	11.2	0.9987	2.410
Nd	DNI	97	91	86	80	76	11.3	0.9943	2.497

Moreover, these complexes have been found to be stable at room temperature but, it has been found that when subjected to sudden high temperature they ignite.

Following equation was used by Freeman and Gorden [40] to evaluate the pre-ignition reactions:

$$dQ_H/dt = d_H/dt - dq/dt \quad (6)$$

where dQ_H/dt is the net rate of heat gain in the system, d_H/dt is the rate of heat produced by pre-ignition reactions, dq/dt is the rate of heat dissipation. They used the above equation and established the following equation which correlates ignition delay i.e., t_{id} , heat of activation and temperature [40]

$$t_{id} = Ae^{\Delta H^*/RT} \quad (7)$$

where ΔH^* is the heat of activation and is approximately equal to activation energy (E^*). If the activities of the reactants do not change significantly during pre-ignition reactions, the log of the time of ignition should be a linear function of the reciprocal of the absolute temperature and the relation comes out to be as given in Eq. (7).

In addition evolution of gases takes place before ignition and reddish brown (CeO_2), dark reddish brown (Pr_6O_{11}), and light blue color (Nd_6O_{11}) solid residues are left in the ignition tubes. Values of ignition delay and activation energies for ignition in the temperature range 350–430 °C are tabulated in Table 5. Here, the values of energy of E^* for Ce, Pr, and Nd complexes are, respectively, 11.5, 11.2, and 11.3 kJ mol⁻¹. Ignition becomes inconsistent (no flame appears i.e., do not ignite) before 350 °C (Table 5). The ignition delay depends exponentially on temperature (as mentioned in Eq. 7). On the basis of these assumptions a plot of $\ln t_{id}$ against $1/T$ has been made which is depicted in Fig. 13. The process of ignition [41] can never be treated as steady-state, since it is a transient process before sustained combustion. It is obvious that these values of activation energies are almost equal and there is no any significant difference among E^* for all the complexes. But E_a values obtained from the kinetic analysis in the temperature range 230–290 °C suggest that there could be thermal stability order. Henceforth, on the basis of these activation energy values (obtained from the kinetic analysis) the thermal stability of praseodymium complex is more than the cerium complex and this in term is stable than neodymium complex. For these complexes difference in the activation energies (E_a) obtained from kinetic analysis is much greater than those obtained from ignition delay (E^*). This is due to the differences in temperatures in both the studies.

Conclusions

Newly prepared cerium and neodymium complexes are nine coordinated, whereas praseodymium complex contains two

type of Pr atom, first is ten coordinated and second is nine coordinated. TG studies show that these follow multistep decomposition to form CeO_2 , Pr_6O_{11} , and Nd_6O_{11} as end product which was confirmed by their XRD patterns. Activation energies obtained from kinetic analysis (E_a for isothermal decomposition) suggest that praseodymium complex was found to be more stable than cerium and neodymium.

Acknowledgements Thanks are due to Head, Chemistry Department, DDU Gorakhpur University, Gorakhpur for lab facilities. The financial assistance UGC for Emeritus Fellow to Dr. Gurdip Singh and CSIR for SRF to Dinesh Kumar is also acknowledged. Authors are also thankful to Institute Instrumentation Centre, IITR, Roorkee for TG-DSC and Chairman, Department of Materials Engineering, IISc, Bangalore for providing XRD facility.

References

- Carmona D, Lamata MP, Oro LA. Recent advances in homogeneous enantioselective Diels–Alder reactions catalysed by chiral transition–metal complexes. *Coord Chem Rev.* 2000;200–202: 717–72.
- Epstein DM, Chapell LL, Khalili H, Supkowski RM, Horrocks WD, Morrow JR Jr. Eu(III) macrocyclic complexes promote cleavage of and bind to models for the 5'-cap of mRNA. Effect of pendent group and a second metal ion. *Inorg Chem.* 2000;39 (10):2130–4.
- Feng J, Sun G, Pei F, Liu M. Comparison between GdDTPA and two gadolinium polyoxometalates as potential MRI contrast agents. *J Inorg Biochem.* 2002;92:193–9.
- Sessler JL, Miller RA. New drugs with diverse clinical applications in radiation and photodynamic therapy. *Biochem Pharmacol.* 2000;59:733–9.
- Ulusoy U, Whitley JE. Determination of intestinal uptake of iron and zinc using stable isotopic tracers and rare earth markers. *Nutr Res.* 1999;19(5):675–88.
- Agwara MO, Ndifon PT, Ndikontar MK. Physicochemical studies of some hexamethylenetetramine metal(II) complexes. *Bull Chem Soc Ethiopia.* 2004;18:143–8.
- Xuan YW, Wu W, Li SJ. Synthesis and crystallographic characterization of a six coordinate Cu(II) complex based on hexamethylenetetramine ligand. *Cryst Res Technol.* 2009;44:127–30.
- Li F, Ma J, Song S, Yang J, Liu Y, Su Z. Influence of neutral ligands on the structures of silver(I) sulfonates. *Inorg Chem.* 2005;44:9374–83.
- Zheng Y, Ying E. Malonato-bridged hexamethylenetetramine coordination polymers containing Mn(II) and Cu(II). *J Coord Chem.* 2005;58(5):453–60.
- Lim MJ, Murray CA, Tronic TA, deKrafft KE, Ley AN, deButts JC, Pike RD, Lu H, Patterson HH. Copper(I) cyanide networks: synthesis, structure, and luminescence behaviour. Part 2. Piperazine ligands and hexamethylenetetramine. *Inorg Chem.* 2007;47: 6931–47.
- Larionov SV, Kokina TE, Glinskaya LA, Klevtsova RF. Nickel(II) diisobutylidithiophosphinate complexes with hexamethylenetetramine and triethylenediamine: synthesis and properties. Crystal and molecular structure of $[Ni_2(C_6H_{12}N_4)\{i-C_4H_9\}_2 PS_2]_4$. *Russ J Coord Chem.* 2002;28(8):560–4.
- Zhang Y, Li J, Nishiura M, Imamoto T. Structural, spectral and thermal properties of a new anion zinc(II) hexamethylenetetramine complex. *J Mol Struct.* 2002;523:257–60.

13. Liittringhauusn A, Kullick W. Gemischte carbonyl komplexe des Cr⁰ und des Mo⁰ mit organo-stickstoffverbindungen. *Tetrahedron Lett.* 1959;10:13–5.
14. Zheng S, Tong M, Chen X. Silver (I)–hexamethylenetetramine molecular architectures: from self-assembly to designed assembly. *Coord Chem Rev.* 2003;246:185–202.
15. Xue H, Gao H, Twamley B, Shreeve JM. Energetic nitrate, perchlorate, azide and azolate salts of hexamethylenetetramine. *Eur J Inorg Chem.* 2006;15:2959–65.
16. Cheng C, Gong S, Fu Q, Shen L, Liu Z, Qiao Y, Fu C. Hexamethylenetetramine as both a ligand and a reducing agent in AGET atom transfer radical batch emulsion polymerization. *Polym Bull.* 2011;66:735–46.
17. Sieranski T, Kruszynski R. Magnesium sulphate complexes with hexamethylenetetramine and 1,10-phenanthroline—thermal, structural and spectroscopic properties. *J Therm Anal Calorim.* 2012;109:141–52.
18. Konar S, Mukherjee PS, Drew MGB, Ribas J, Chaudhari NR. Synthesis of two new 1D and 3D networks of Cu(II) and Co(II) using malonate and urotropine as bridging ligands: crystal structures and magnetic studies. *Inorg Chem.* 2003;42:2545–52.
19. Dalvi AA, Satpati AK, Palrecha MM. Simultaneous determination of Pt and Rh by catalytic adsorptive stripping voltammetry, using hexamethylenetetramine (HMTA) as complexing agent. *Talanta.* 2008;75:1382–7.
20. Fedoroff BT, Sheffield OE. *Encyclopedia of explosives and related items*, vol. 5. Dover: Picatinny Arsenal; 1966. p. E95.
21. Koper JH, Jansen OG, van den Berg PJ. Delft Technische Hogeschool. Netherlands: *Explosivstoffe*; 1970. p. 181–3.
22. Singh G, Kapoor IPS, Pandey DK. Hexamine metal perchlorates as energetic burning rate modifiers. *J Energ Mater.* 2002; 20:223–44.
23. Singh G, Pandey DK. Studies on energetic compounds, part 27: kinetics and mechanism of thermolysis of bis(ethylenediamine) metal nitrates and their role in the burning rate of solid propellants. *Propellants Explos Pyrotech.* 2003;28(5):231–9.
24. Singh G, Barnawal BP, Kapoor IPS, Kumar D, Singh CP, Frohlich R. Preparation, X-ray crystallography and thermal decomposition of some transition metal nitrate complexes with hexamethylenetetramine. *J Therm Anal Calorim.* 2008;91(3): 971–7.
25. Singh G, Barnawal BP, Kapoor IPS, Kumar D, Frohlich R. Preparation, X-ray crystallography and thermal decomposition of some transition metal perchlorate complexes with hexamethylenetetramine. *J Phys Chem A.* 2007;111:12972–6.
26. Singh G, Shrimal AK, Kapoor IPS, Singh CP, Kumar D, Mannan SM. Kinetics of thermolysis of some transition metal perchlorate complexes with 1,6-diaminohexane ligand. *J Therm Anal Calorim.* 2011;103:149–55.
27. Singh G, Singh CP, Fröhlich R. Preparation, characterization and thermolysis of metal nitrate complexes with 4,4'-bipyridine. *J Therm Anal Calorim.* 2006;85:425–31.
28. Kumar D, Kapoor IPS, Singh G, Goel N, Singh UP. Preparation, X-ray crystallography and thermolysis of transition metal nitrates of 2,2'-bipyridine. *J Therm Anal Calorim.* 2012;107:325–34.
29. Kumar D, Kapoor IPS, Frohlich R, Singh G. Preparation, characterization, and kinetics of thermolysis of nickel and copper nitrate complexes with 2,2'-bipyridine ligand. *Thermochim Acta.* 2012;545:67–74.
30. Trzesowsk-Kruszynska A, Kruszynski R, Zalewicz M, Bartczak TJ. Coordination sphere geometry changes of lanthanoid(III)nitrate complexes with hexamethylenetetramine. *J Coord Chem.* 2010;63(6):1013–28.
31. Sheldrick GM. SADABS, Program for scaling and correction of area detector data. Göttingen: University of Göttingen; 1996.
32. Sheldrick GM. Phase annealing in SHELX-90: direct method for larger structures. *Acta Crystallogr A.* 1990;46:467–73.
33. Sheldrick GM. SHELXTL-NT, version 6.12. Reference manual. Göttingen: University of Göttingen; 2000.
34. Klaus B. DIAMOND, version 1.2c. Bonn: University of Bonn; 1999.
35. Allen FH. The Cambridge structural database: a quarter of a million crystal structures and rising. *Acta Crystallogr B.* 2002;58:380–8.
36. Singh G, Singh RR. Indigenously fabricated apparatus for thermogravimetric analysis. *Res Ind.* 1978;23:92–3.
37. Brown ME, Dollimore D, Galway AK. Reactions in the solid state, comprehensive chemical kinetics, vol. 22. Amsterdam: Elsevier; 1977. p. 1–340.
38. Vyazovkin S, Wight CA. Isothermal and nonisothermal reaction kinetics in solids: in search of ways toward consensus. *J Phys Chem A.* 1997;10:8279–84.
39. Singh G, Kapoor IPS, Vasudeva SK. Thermolysis of AP-PS-additive mixtures. *Indian J Technol.* 1991;29:584–9.
40. Freeman ES, Gorden S. The application of the absolute rate theory of the ignition of propagatively reacting systems: thermal ignition of the system, lithium nitrate–magnesium, sodium nitrate–magnesium. *J Phys Chem.* 1956;60:867–71.
41. Zinn J, Rogers RN. Thermal initiation of explosives. *J Phys Chem.* 1962;66:2646–53.